AGEING BEHAVIOUR OF COMPOSITE ROCKET PROPELLANT FORMULATIONS

S. Cerri* **, M.A. Bohn*, K. Menke*, L. Galfetti**

*Fraunhofer Institut fuer Chemische Technologie (ICT)
Postfach 1240, D-76318, Pfinztal-Berghausen, Germany

**SPLab, Dipartimento di Ing. Aerospaziale, Politecnico di Milano
Via La Masa 34, I-20156, Milan, Italy

Abstract

Several HTPB/AP propellant formulations differing in the aluminium particle size (microAl vs. nanoAl) have been manufactured freshly and investigated in unaged and aged conditions. All the formulations contain 16 mass-% of binder, consisting of HTPB-IPDI, plasticizer and antioxidant. Two families of materials having 6 mass-% and 12 mass-% of Al content were compared. The nanoaluminium content was limited to 6 mass-%. The ballistic performances of the propellant formulations were calculated using the ICT-Thermodynamic code. EDX analyses of the unaged materials and SEM analyses of the unaged and aged materials were made. Uniaxial tensile tests have been conducted at room temperature using three different strain rates. DMA analyses in torsion mode and DSC measurements were performed with the purpose to investigate changes in the glass transition temperatures of the materials during ageing. A discussion of the factors influencing the loss factor of the material is presented and an explanation on the molecular level is given.

INTRODUCTION

HTPB-based rocket propellant formulations are currently and widely used in propellant boosters. They have a 3-dimensional polyurethane network which acts in binding rigid oxidiser particles (ammonium perchlorate) and metal powders (mainly aluminium). From the manufacturing process to the effective use of the propellant inevitably a natural ageing occurs. Especially the binder is the weak part of the formulation. It is very sensitive to ageing phenomena mainly due to the oxidative ageing. Oxidation is a chemical reaction leading to free radicals which can start chain reactions involving chain propagation and chain branching and damage the material by their occurrence. Therefore in order not to eliminate but to slow down these damaging reactions of the binder an antioxidant is added to the mixture during manufacturing. This substance inhibits the chain reactions by removing the free radical intermediates by H radical transfer and forming a more stable radical and finally is oxidised itself. Several chemical, physical and mechanical processes occur during ageing leading to a reduction of the in-service time of the solid rocket motors. In order to simulate the long-term ageing of the material within a reasonable time, the propellant specimens are accelerated aged at temperatures higher than the ambient temperature. To establish ageing conditions equivalent in thermal load to the in-service ageing the Arrhenius expression based time-temperature scaling can be applied, Eq.(1).

$$t_E(T_E) = t_T(T_T) \cdot \exp\left[-\frac{E_a}{R} \cdot \left(\frac{1}{T_T} - \frac{1}{T_E} \right) \right] \quad (1)$$

t_E = time at the in-service temperature T_E;
t_T = test-time at the test temperature T_T;
E_a = activation energy [kJ/mol];
R = general gas constant [J/mol·K].

By knowing the activation energy of the material and fixing the in-service time of the system (10 or 20 years at 25°C) an ageing programme can be planned in principle. But some points have to be

emphasized. Firstly, the value of the activation energy is the final output of an ageing programme. Secondly, the ageing kinetic does not always obey the single Arrhenius law as evidenced in the work of Celina a.o. in the case of polybutadiene [1]. Finally, in the research and development of new energetic formulations efforts are involved aiming on higher ballistic and mechanical performances. In a well-established formulation every new ingredient added can modify the ageing behaviour of the final cured propellant in a non-predictable way. In order to define an ageing programme in terms of time-temperature load, using appropriate time ranges, an empirical formula based on the generalized van´T Hoff rule could be applied (Eq. 2). This formula has a special characteristic: it simulates quite well a two step decomposition mechanism often found with energetic material and also with HTPB binder oxidation. The relation between the factor F and the Arrhenius expression and the use of two step mechanistic description are explained in detailed in the paper of Bohn [2].

$$t_E[y] = t_T[d] \cdot F^{\frac{T_T - T_E}{\Delta T_F}} \cdot \frac{1}{365.25} \qquad (2)$$

t_E = time in years at the in-service temperature T_E; t_T = test time in days at the test temperature T_T;
F = reaction rate change factor per 10°C of temperature change, usually its value is between 2 and 5;
ΔT_F = temperature interval for actual value of F (10°C was used here). T_T and T_E are both in °C.

The value of the factor F is a function of the activation energy of the ageing process. A value of F = 2.5 was used in this study to establish the ageing plan. The thermal accelerated ageing programme was carried out in PID temperature-controlled (± 0.5°C) ageing ovens (design from former company Julius Peters, Berlin) in order to investigate the ageing of the surface-layer of solid rocket propellants. Specimens were aged at 60°C (75 days, 150 days, 220 days), 70°C (30 days, 60 days, 90 days), 80°C (12 days, 25 days, 40 days) and 90°C (5 days, 10 days, 15 days) in air (RH < 10%) to simulate 15 years of natural ageing at 25°C.

FORMULATIONS

Four aluminised HTPB/AP-based rocket formulations having a solid load of 84 mass-% have been manufactured freshly. All the formulations contain 16 mass-% of binder, consisting of HTPB R45M™ (10.72 mass-%), IPDI (0.89 mass-%), plasticizer (DOA, 4 mass-%) and antioxidant (Irganox™ 565, 0.2 mass-%). In order to improve the mechanical properties a bonding agent was added to the formulation (HX-878, 0.19 mass-%). The NCO/OH equivalent ratio was set to 0.87. As catalyst for the curing reaction 0.02 mass-% of Triphenylbismuth (TPB) was added. All the formulations were prepared in a vertical kneader (Drais T FHG, Germany) having a volume of 5 l and were cured in an electrical oven cabinet (company Memmet, Germany) for two days at 60°C. Two families of materials having 6 mass-% (AV03 18 µm, AV05 100-200 nm) and 12 mass-% (AV04 18 µm, AV06 6 mass-% 100-200 nm and 6 mass-% 18 µm) of aluminium content were compared. In order not to get too high values of casting viscosity [3, 4] the nano-aluminium content was limited to 6 mass-%.

THERMODYNAMIC CALCULATIONS

The rocket propellant formulations chosen for the ageing programme were also analysed with the ICT-Thermodynamic Code and the ICT Thermochemical Database. The thermodynamic equilibrium in the nozzle was calculated at constant pressure with an expansion ratio of 70:1 (EU standard condition). The ballistic performances, the gravimetric specific impulse (I_{sp}), the volumetric specific impulse (I_{spv}) and the vacuum specific impulse ($I_{spvacuum}$), were obtained in frozen equilibrium and equilibrium flow. Only the parameters of the second condition are reported here.
The experimental formulations contain different sizes of the aluminium powder: nanoAl vs. microAl. From a thermodynamic point of view both powders are identical. It is widely known that the aluminium particles are covered by an amorphous porous layer named alumina (Al_2O_3). Several researchers [5, 6]

have measured its thickness and a good representative value is seen as 3-4 nm. The mass fraction of this layer becomes remarkable when moving from the micrometric particles to the nanometric ones. Therefore, by considering the value of the active aluminium (Al^0) of the powders indirectly the average size of the particles can be taken into account. The calculations show the evolution of the parameters considering materials having a 16 mass-% of binder (HTPB R45M™, DOA, IPDI, TPB, Irganox™ 565) and a 84 mass-% of solid load (AP+Al). The enthalpy of formation of the bonding agent used was unknown, hence as a solution with an acceptable error, the mass fraction of this component was added to the mass fraction of the prepolymer (HTPB R45M™). To study the impact of the metal powders, an aluminium sweep from 0 mass-% to 18 mass-% was done. Three formulations were investigated: propellant with only micrometric aluminium inside, propellant with only nanoAl and propellant having a mixture of nanoAl and microAl. The nano aluminium powders having only an alumina layer (also called uncoated powders) are very susceptible to ageing. So, under strong accelerated ageing conditions (high temperature and high relative humidity values) the powders degrade rapidly [7, 8] giving $Al(OH)_3$ and not Al_2O_3 as shown in several papers [3, 7, 9]. The values used for the calculations are reported in Table 1 and were taken from the paper of Cliff a.o. [7]. The performance calculations were done making an Al^0 sweep, whereas the alumina content was kept constant, which implies that the decrease of Al^0 has only formed $Al(OH)_3$.

Table 1: Contents of active aluminium (Al^0), alumina (Al_2O_3) and bayerite ($Al(OH)_3$) of the investigated formulations.

Propellants	Unaged condition		Aged condition		
	Al^0 [mass-%]	Al_2O_3 [mass-%]	Al^0 [mass-%]	Al_2O_3 [mass-%]	$Al(OH)_3$ [mass-%]
AV03	5.976	0.024	4.350	0.024	1.626
AV04	11.952	0.048	0.240	0.048	3.252
AV05	5.292	0.708	8.700	0.708	5.052
AV06	11.268	0.732	4.590	0.732	6.678

The propellant formulations containing unaged aluminium show an increase in the ballistic performance by adding more metal particles inside the mixture. Therefore, the materials with microAl have the highest Al^0 content and show the highest ballistic quantities. Then the materials with the mixture and finally the propellant containing only nanoAl follow. So, from a thermodynamic point of view the use of nano aluminium is not so advantageous as might be expected due to the lower aluminium content.

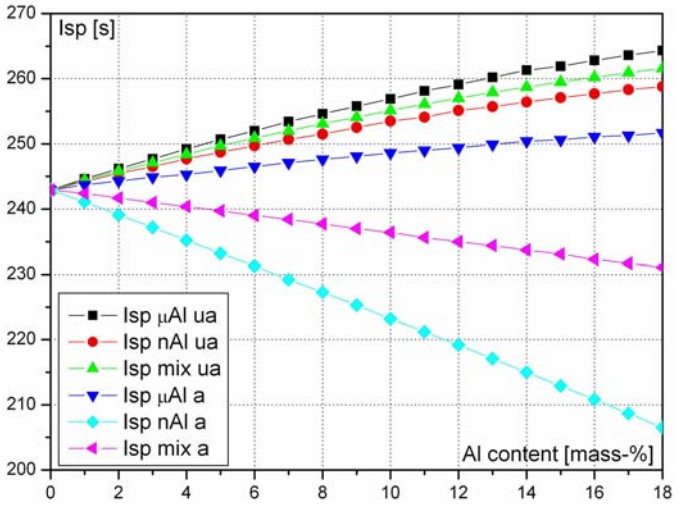

Figure 1: Gravimetric specific impulse (I_{sp}) vs. aluminium solid load of formulations containing aged and unaged powders.

By considering the aged formulations only the one containing microAl evidences a monotonic increase of the performances with the mass-% of Al, whereas the ones having nanoAl inside show a remarkable decrease of the performances due to the increasing presence of inert masses (Al_2O_3 and $Al(OH)_3$). In all cases a decrease of the performances with respect to the unaged situation is clearly shown in Table 2. The presence of aged aluminium has an impact on the theoretical density of the propellants (Table 3). The reduction of Al^0 with ageing affects also the efficiency of the combustion process causing a reduction in the flame temperature and an increase of the two-phase flow losses (presence of more solid particles in the combustion gases).

Table 2: Compilations of the losses in the parameters using aged aluminium inside the formulations.

Propellants	I_{spA*}/I_{spUA**} [%]	$I_{spvacuumA}/I_{spvacuumUA}$ [%]	I_{spvA}/I_{spvUA} [%]	$T_{chamberA}/T_{chamberUA}$ [%]
AV03	2.18	2.28	2.29	3.89
AV04	3.74	3.99	3.98	6.96
AV05	7.41	7.71	7.75	13.20
AV06	8.48	8.93	8.91	15.58

*A = aged condition
**UA = unaged condition

Table 3: Theoretical density values of the unaged and aged formulations.

Propellants	ρ_{thUA} [g/cm^3]	ρ_{thA} [g/cm^3]	1- ρ_{thA}/ρ_{thUA}
AV03	1.693	1.691	0.12
AV04	1.718	1.714	0.23
AV05	1.696	1.689	0.41
AV06	1.721	1.712	0.52

EXPERIMENTAL TECHNIQUES

Tensile tests and EDX analyses were done only for the unaged samples. JANNAF dog-bone specimens (125x25x10/12 mm) were tested in uniaxial tensile test at room temperature and atmospheric pressure at three constant strain rates (0.00167 s^{-1}, 0.0167 s^{-1}, 0.167 s^{-1}) using the ZWICK UPM 1476 tensile machine. During this measurement the propellant specimen is ruptured and part of the fracture surface was cut out in order to investigate its morphology with SEM and the dispersion level of the aluminium particles with EDX mapping analyses using the scanning electron microscope Supra 55 VP manufactured by Zeiss, Germany. EDX mapping was done only with material subjected to the highest strain rate, whereas SEM images were taken from samples at all applied strain rates. A series of SEM analyses was done also with aged mini dog-bone samples, aged at 90°C with the purpose to investigate possible dewetting phenomena. The dynamic mechanical behaviour of the aged samples was examined in torsion mode using a DMA instrument of type ARES (Advanced Rheometric Expansion System) manufactured by the former Rheometric Scientific Inc. Piscataway, New Jersey, USA. A liquid-nitrogen cooling accessory was used for the low temperature measurements but applied also at positive temperatures because of better temperature control. The specimens used were small rectangular bars (50x10x4/5 mm). The temperature range for the frequency-temperature sweep analyses was -100°C to 70°C, with the heating rate of 1 °C/min and the soak time of 28 s. The samples were tested at four frequency values (0.1, 1.0, 10.0, 56.0 Hz) using a strain control with maximum strain of 0.0012 in order not to damage the material. The measurement reproducibility is high. Therefore, only one sample per each test condition was measured. Only if anomalous behaviours have occurred a second measurement was performed.

RESULTS AND DISCUSSIONS

The mechanical properties of the propellants were evaluated in terms of corrected stress, logarithmic strain, stiffness at 2.5% of strain and rupture energy, but only the previous two parameters are here reported. In any case all the quantities have revealed an increase by increasing the strain rate. The even-numbered formulations achieved higher strength values. The use of nanometric aluminium gives an increase in the corrected stress due to the high specific surface. Figure 2 shows that with the use of a mixture containing nanoAl and spherical microAl the propellant achieves good mechanical properties, but not with the use of only nano powder.

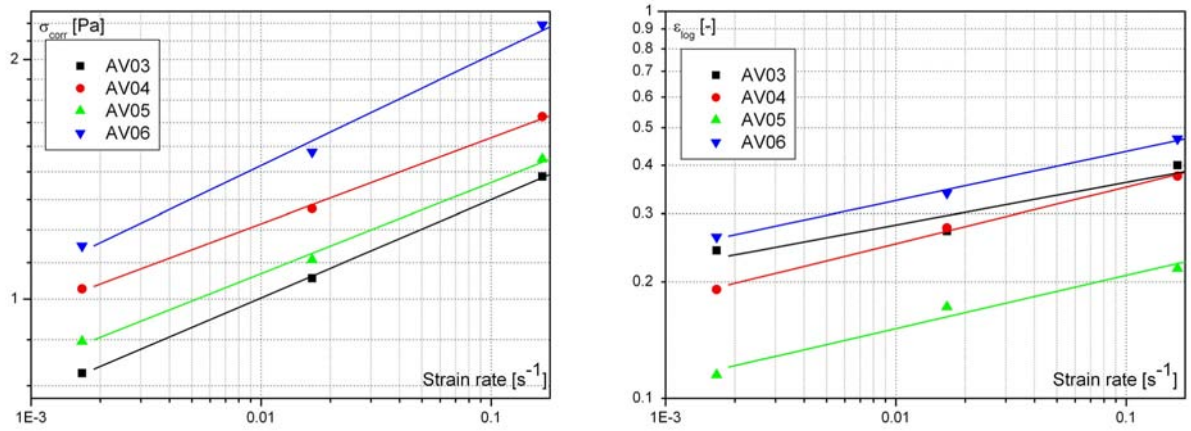

a) b)

Figure 2: a) Bi-logarithmic plot of the corrected stress vs. strain rate; b) Bi-logarithmic plot of the logarithmic strain vs. strain rate.

SEM images of the aged and unaged propellants have not shown the presence of voids or visible dewetting phenomena. The EDX mapping micrographs of the element Al (Figure 3a-d) underline that the propellants containing nanoAl have a high dispersion level of these particles. During the kneading nanoAl can be distributed in a homogeneously way within the soft binder. The use of higher magnifications has pointed out the presence of nearly perfect spherical micrometric aggregates of nanoAl (Figure 3e), formed during kneading.

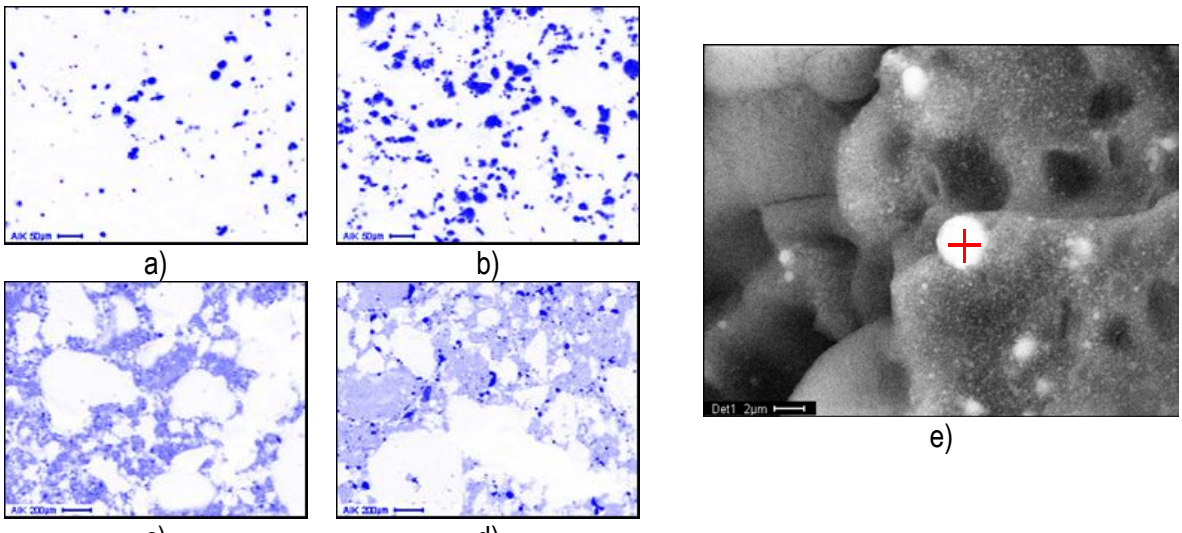

a) b) c) d) e)

Figure 3: EDX analyses of the unaged propellants tested with the highest strain rate (0.167 s^{-1}): a) AV03; b) AV04; c) AV05; d) AV06; e) EDX analysis at high magnification for propellant AV05.

DMA measurements describe the dynamic mechanical behaviour of the propellant using three main quantities: storage modulus (G'), loss modulus (G") and loss factor (tan(δ)). The trend of the loss factor with ageing is shown in Figure 4. For every ageing condition the presence of two maxima can be seen. The first maximum is frequency dependent. It is located between -80°C and -60°C (depending on the applied frequency) and is attributed to the main glass transition of the HTPB main chain elements, which are called also soft-segment units, where the main chain molecular motion ceases or starts. Here some molecular rearrangements occur and the polymeric material changes from the entropy-elastic rubber behaviour to the energy-elastic glass behaviour. The centre temperature of the change is called glass transition temperature $T_g^{unrestricted}$. The values agree with those obtained with DSC measurements (Table 4) and are only slightly influenced by ageing.

Table 4: Glass transition temperatures evaluated for aged and unaged propellants.

Propellants	$T_g^{unrestricted}$ unaged [°C]	$T_g^{unrestricted}$ (90°C, 15 days) [°C]	$T_g^{unrestricted}$ (80°C, 40 days) [°C]	$T_g^{unrestricted}$ (70°C, 60 days) [°C]
AV03	-83.05	-82.93	-80.93	-81.26
AV04	-82.87	-82.93	-82.17	-81.81
AV05	-81.67	-83.71	-82.66	-82.06
AV06	-82.14	-83.11	-82.20	-82.77

The second maximum is also frequency dependent and is broader than the first one. It appears at higher temperatures and is related to the motions within the so-named short hard-segment units or mobility restricted soft-segments regions. This restriction leads to higher glass transition temperatures of these segments, called $T_g^{restricted}$, and it is assumed that they are caused by the binder filler-interactions [10-13]. The different nature of these two relaxation phenomena can be seen also considering the apparent activation energy obtained from the shift with frequency of the temperatures of the maxima [14].

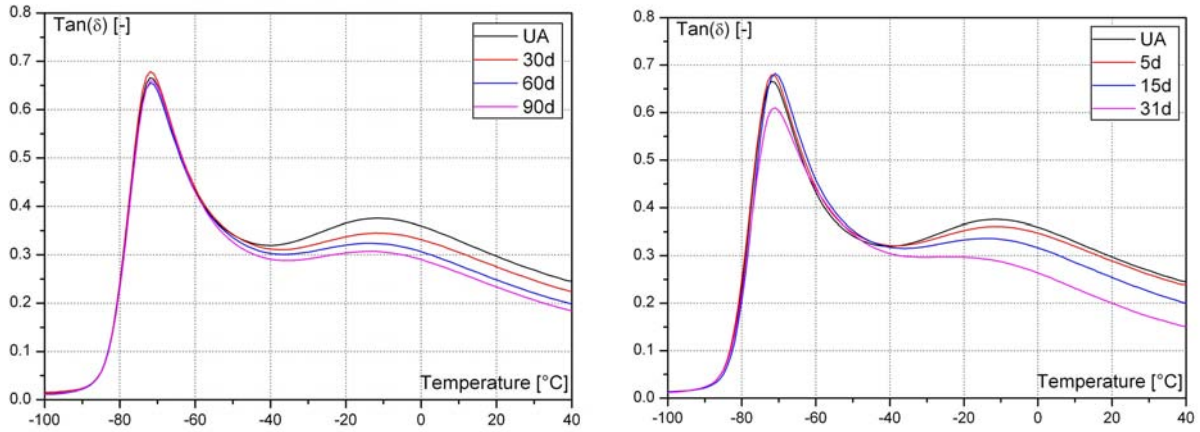

a) b)

Figure 4: Loss factor vs. temperature at different ageing time for the aged AV04: a) 90 °C; b) 70 °C.

A schematic qualitative representation, a model picture, of the different binder regions influencing the behaviour of the loss factor is given in Figure 5a. The propellant is constituted by a soft matrix having inside HTPB main chain elements cross-linked by the curing agent, here IPDI. HTPB has a functionality of somewhat >2 but the NCO/OH ratio of the material was 0.87. This means that some free chains (not linked chains) are within the cured material. The propellant has also rigid fillers inside (oxidiser+metal particles) that enhance the mechanical properties due to the well known reinforcing effect, means by a type of van-der-Waals interaction between polymer chains neighbouring to particles, thereby reducing

the mobility of these chains. The HTPB main chains are the mobility undisturbed polymer chains between the cross-linking points. During the mechanical/thermal load of the frequency/temperature sweep these chains are at first able to make the molecular rearrangements. However, the filler creates a sort of shell [15] in the binder (HTPB main chains and/or free chains and/or plasticizer) around the particles. In this shell the binder has a restricted mobility and shows the relaxation phenomena (reorientation) at higher temperatures. Also the cross-linking zones influence the mobility of such parts of the polymer chains, which are nearby. Therefore in the polymer binder three zones of different mobility occur together: the (i) main polymer chains, (ii) cross-linking zones, (iii) binder-filler interaction zone.

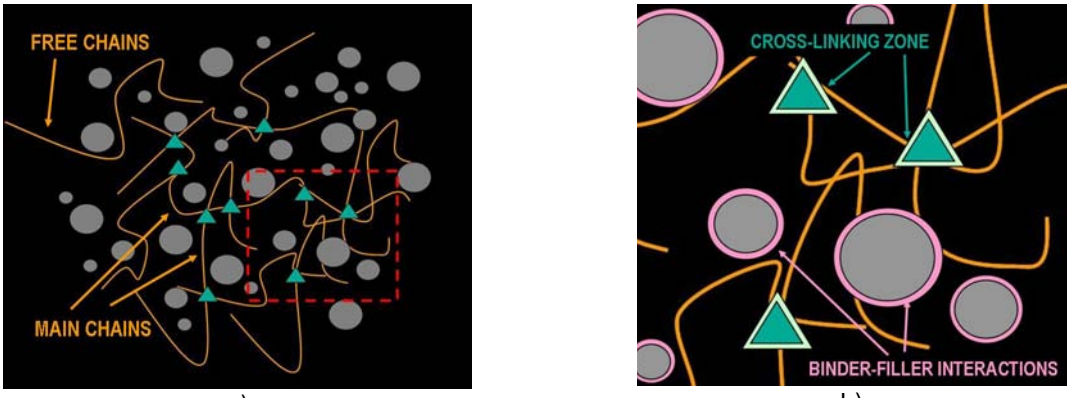

a) b)

Figure 5: Qualitative representation of the different mobility regions influencing the tan(δ). a) Scheme of the propellant structure; b) Magnification of the red area in order to focus on the binder-filler interaction and on the cross-linking zone.

Regarding the first peak, the behaviour of the aged and unaged propellant is quite similar. Figure 4 pointed out that changes are remarkable considering the second peak. The values of tan(δ) are reduced with the ageing time. The area under the curves is reduced too and it is related to the ability of the material to use energy for the molecular rearrangements. In order to evaluate this decrease in area, the experimental data have to be corrected first with the use of a baseline (Eq. 3) applied in a suitable temperature range [T_a, T_b]. The parts not considered by this procedure are such which are caused by only energy dissipation without any useful rearrangement effect, as a type of friction between matrix and filler particles. Figure 6a shows the behaviour of tan(δ) up to temperatures where degradation effects in the material start. At all the frequencies analysed the curves show two plateaus at low and high temperature where tan(δ) has constant values. The temperature values of these plateaus were assigned to T_a and T_b. The baseline corrections were done with Eq.(3) for the curves loaded at 0.1 Hz with baseline setting at: T_a = -99°C, T_b = 69°C.

$$BL(T) = \left[1 - \frac{(T - T_a)}{T_b - T_a} \cdot \tan(\delta(T_a))\right] + \frac{(T - T_b)}{T_b - T_a} \cdot \tan(\delta(T_b)) \quad (3)$$

T_a = lower baseline setting temperature [°C];
T_b = upper baseline setting temperature [°C];
$\tan(\delta(T_a))$ = value of tan(δ) at T_a [-];
$\tan(\delta(T_b))$ = value of tan(δ) at T_b [-];

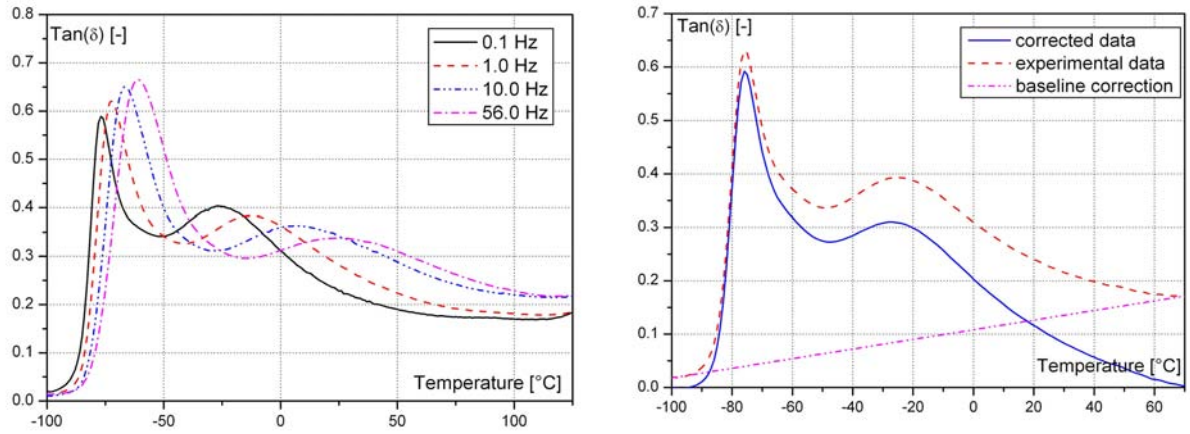

a) b)

Figure 6: a) Loss factor vs. temperature at different frequency values until the decomposition processes start to occur; b) Comparison between original data and data having the baseline corrections.

After the baseline corrections several fitting functions were analysed in order to find the most appropriate one. Here three fitting equations are reported and the peculiar parameters are also explained. Eq. 4: EMG model (Exponentially Modified Gaussian, created by convolution between an exponential function and a Gaussian distribution); Eq. 5: Gaussian model; Eq. 6: Gauss lognormal model.

$$\tan(\delta) = td_0 + \sum_{i=1}^{N} \frac{A_i}{\tau_i} \cdot \frac{1}{2} \cdot \exp\left[0.5 \cdot \left(\frac{w_i}{\tau_i}\right)^2 - \frac{T - Tc_i}{\tau_i}\right] \cdot \left\{1 - \mathrm{erf}\left[-\frac{1}{\sqrt{2}} \cdot \left(\frac{T - Tc_i}{w_i} - \frac{w_i}{\tau_i}\right)\right]\right\} \quad (4)$$

$$\tan(\delta) = td_0 + \sum_{i=1}^{N} \frac{A_i}{w_i \cdot \sqrt{2\pi}} \cdot \exp\left[-0.5 \cdot \left(\frac{T - Tc_i}{w_i}\right)^2\right] \quad (5)$$

$$\tan(\delta) = td_0 + \sum_{i=1}^{N} \frac{A_i}{(T + Ts) \cdot w_i \cdot \sqrt{2\pi}} \cdot \exp\left[-0.5 \cdot \left(\frac{\ln(T + Ts) - \ln(Tc_i + Ts)}{w_i}\right)^2\right] \quad (6)$$

T = measurement temperature [°C];
tan(δ) = value of tan(δ) as function of T [-];
A = peak area of total EMG peak, also equivalent of area of Gauss peak alone [°C];
w = half peak width at half height of only Gaussian part [°C];
Tc = temperature at peak maximum in the Gaussian part of EMG (not the peak maximum of EMG) [°C];
Ts = shift constant to shift the T axis to more positive values (condition: $Tc_i+Ts>0$, $Ts>-Tc_i$)
τ = relaxation parameter in exponential part of EMG, $f_E(T) = \exp(-T/\tau)$;
td_0 = offset in tan(δ) data [-];
N = number of fitting functions;
erf in EMG means the error function

The use of a non suitable fitting model has two drawbacks: it is not possible to evaluate correctly the area under the second peak; it is not possible to compare the "weight" of the second peak with respect to the first one. Figure 7a shows the fitting curve of the three models given above with N=2. The Gauss model achieves only a poor description of the experimental data, whereas the EMG and the Gauss lognormal model are quite good but both cannot describe well the valley region between the two maxima. In Figure 7b a peak separation enables to see the single EMG curves of the main and of the second peaks.

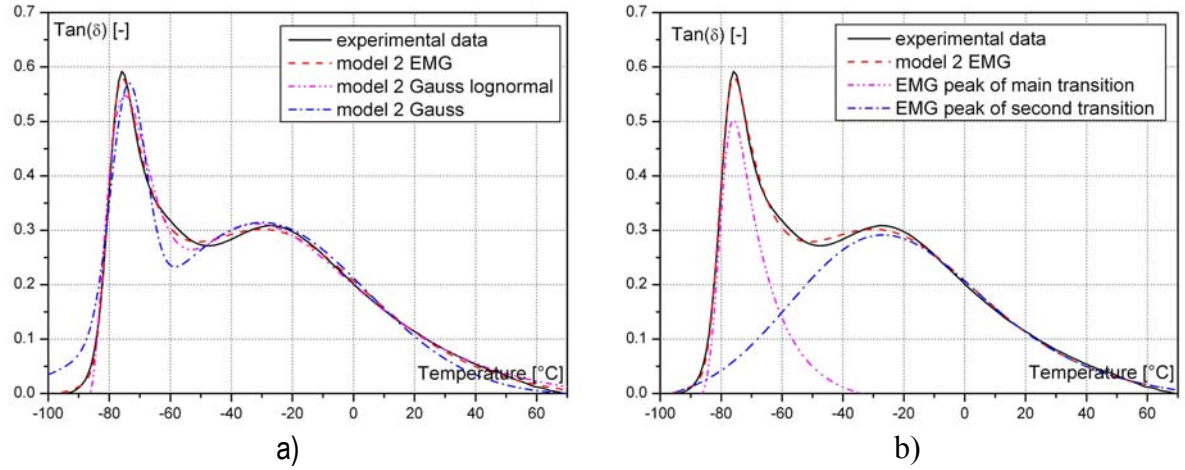

Figure 7: a) Fittings of the loss factor with N=2: EMG model, Gauss model, Gauss lognormal model; b) Peak separation of the total EMG fitted with N=2.

The simulation of the single EMG functions using the fitting parameters obtained with Eq. 4 evidences that the area of the second peak is underestimated (Figure 7b). For this reason an EMG fitting with N=1 was made for a reduced temperature range [-40°C, 70°C]. By plotting the values of the area vs. the ageing days at different ageing temperatures a linear dependence is observed (Figure 8a). By plotting the natural logarithm of the slopes $\ln(k_A)$ of these lines versus 1/T, (where the temperature is in Kelvin) the value of an activation energy is obtained: Ea ~70 kJ/mol (Eq. 7).

$$\ln(k_A) = \ln(Z) - \frac{Ea}{R} \cdot \frac{1}{T} \tag{7}$$

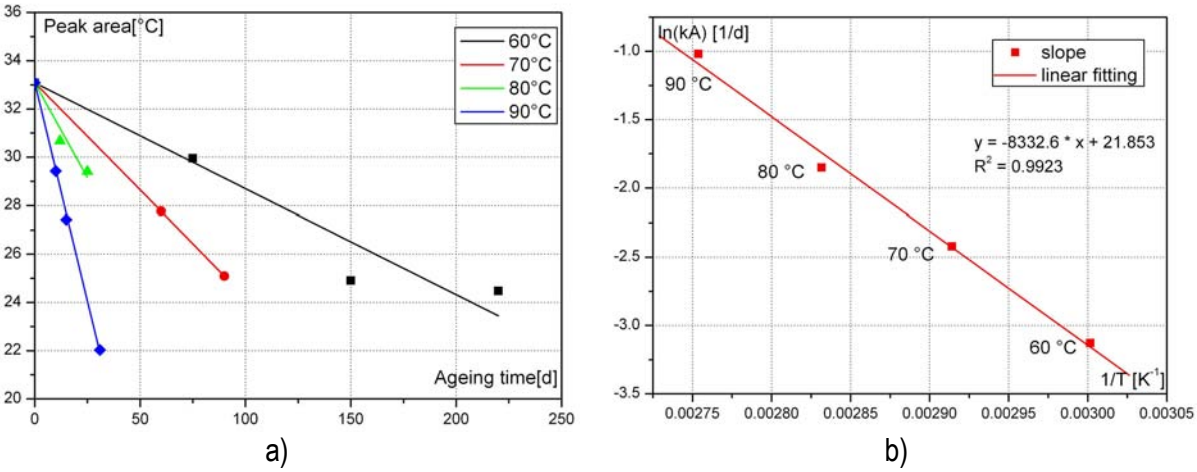

Figure 8: a) Peak area of the second peak using the EMG function with N=1 and a reduced temperature range [-40°C, 70°C]; b) Arrhenius type diagram: linear fitting of slopes of the lines of Figure 8a as $\ln(k_A)$ versus 1/T at different ageing temperatures in order to evaluate the activation energy.

Focusing the attention on the shape of the valley zone seems that another peak, just nearby the first one, is present. Remaking the fittings of the same experimental data using the models with N=3 the curves in Figure 9a are obtained. The Gauss model is again not satisfying in representing the experimental data well but the EMG and Gauss lognormal gives good descriptions. Now the question is which of both is the better fitting function that has to be used to describe the loss factor? Both represent the experimental values (corrected with the baseline function) quite well, but the Gauss lognormal

function must be applied with the shift parameter Ts, which is difficult to interpret. For this reason the choice has to be the EMG function. Figure 9b shows the detail of the EMG fitting. The three peaks are clearly visible and the relative weight also. The EMG peaks of the first (N=1) and third (N=3) function constitute mainly the main peak of the loss factor. The EMG peak of the N=2 function describes the second transition. The presence of these contributions recalls the schematic representation of the three different mobility regimes determining the behaviour of the loss factor shown in Figure 5. The EMG peak of the first peak can be related to the relaxation processes of the HTPB main chains, the EMG peak of the second peak to the reduced mobility of the polymer due to the binder-filler interactions and finally the EMG peak of the third transition can be associated with the relaxation phenomena of the polymer chains nearby the cross-linking zone.

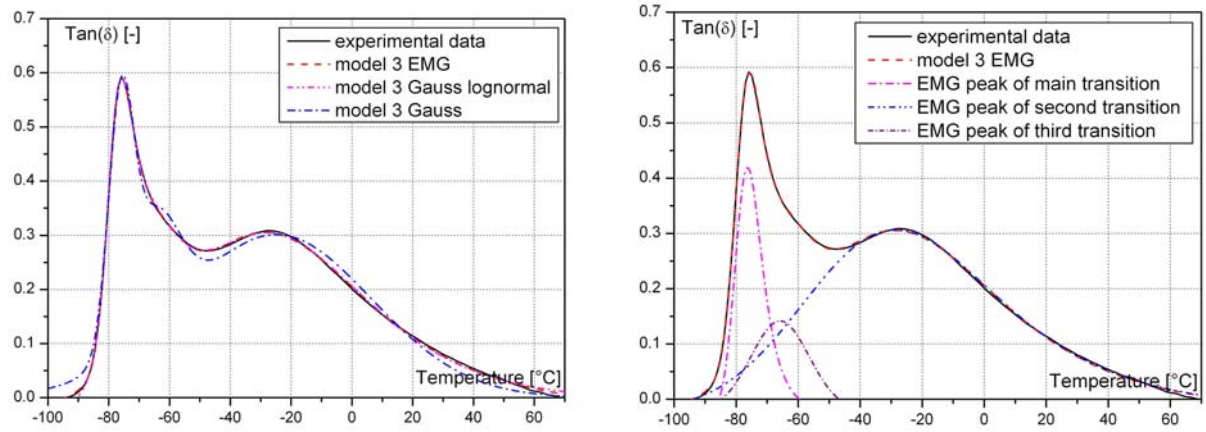

a) b)

Figure 9: a) Fittings of the loss factor with N=3: EMG model, Gauss model, Gauss lognormal model; b) Peak separation of the EMG fitting with N=3.

CONCLUSIONS

Several HTPB/AP propellant formulations differing in the aluminium particle size (microAl vs. nanoAl) have been manufactured freshly and investigated in unaged and aged conditions. All the formulations contain 16 mass-% of binder, consisting of HTPB-IPDI, plasticizer and antioxidant. Two families of materials were compared having 6 mass-% and 12 mass-% of Al content. The nanoaluminium content was limited to 6 mass-%. The calculations performed have underlined the importance of the storage conditions and the quality of the motor sealing especially for propellants containing nano-sized powders. All the mechanical quantities obtained by tensile tests have revealed an increment by increasing the strain rate. The even-numbered formulations achieved higher strength values. The use of nanometric aluminium gives an increase in the corrected stress due to the high specific surface of the Al filler. The results have shown that with the use of a mixture containing nanoAl and spherical microAl, and not the use of only nano powders, the propellant achieves good mechanical properties. The nanoAl powder reaches high dispersion level in the formulation but the use of nanosized powders has a drawback because the particles tend to cluster to spherical micrometric aggregates. SEM micrographs have underlined that with ageing the propellants seem not to get voids or show de-wetting phenomena. DMA measurements have pointed out the pronounced presence of two maxima in the loss factor. Some fitting equations have been used in order to find out an explanation. The so-named exponentially modified Gaussian (EMG) appears to be the best. But only two EMG functions could not describe the total tan(δ) curve completely. In fact, the valley between the two well visible peaks could not be represented satisfactorily, so a fitting function comprising 3 EMG was built and the final modelling results perfectly overlapped with the experimental data, which have been baseline corrected. A model picture based on the molecular explanation of these two maxima can be found taking into consideration the different binder situations in the material. During the DMA measurements three different relaxation phenomena

have been revealed: one is related with the main chains of the HTPB, the second is related with the binder-filler interactions and the third one with binder chains around the cross-linking zones. In this picture the binder-filler interaction is mainly responsible for the second peak, whereas the other two phenomena contribute together to the main peak in loss factor.

REFERENCES

[1] Celina M., Gillen K.T., Assink R.A., Accelerated aging and lifetime prediction: Review of non-Arrhenius behaviour due to two competing processes, *Polymer Degradation and Stability*, Vol. 90, pp. 395-404, 2005.

[2] Bohn M.A., Prediction of Equivalent Time-Temperature Loads for Accelerated Ageing to Simulate Preset In-Storage Ageing and Time-Temperature Profile Loads, *Paper 78* in *Proceedings of the 40th International Annual Conference of ICT*, Karlsruhe, Germany, 23-26 June, 2009.

[3] Shalom A., Aped H., Kivity M., The Effect of Burning Rate Catalysts on Composite Propellants Containing Nanosized Aluminum, *Proceedings of the 35th International Pyrotechnics Seminar of the International Pyrotechnics Society*, pp. 687-694, Fort Collins, Colorado, USA, 13-18 July, 2008. Proceedings by IPSUSA Seminars, Inc. 2008, ISBN 0-9755274-4-4.

[4] Bui D.T., Atwood A.I., AtienzaMoore T.M., Effect of Aluminum Particle Size on Combustion Behavior of Aluminized Propellants in PCP Binder, *Paper 27* in *Proceedings of the 35th International Annual Conference of ICT*, Karlsruhe, Germany, 29 June-2 July, 2004.

[5] Gromov A., Ilyin A., Förter-Barth U., Teipel U., Characterization of Aluminum powders: II. Aluminium Nanopowders Passivated by Non-Inert Coatings, *Propellants, Explosives, Pyrotechnics*, 31, pp. 401-409, 2006.

[6] Phung X., Groza J., Stach E.A., Williams L.N., Ritchey S.B., Surface characterization of metal nanoparticles, *Materials and Engineering A*., Vol. 359, pp. 261-268, 2003.

[7] Cliff M., Tepper F., Lisetsky V., Ageing Characteristics of Alex® Nanosize Aluminum, *37th AIAA/ASME/SAE/ASEE Joint Propulsion Conference and Exhibit*, Salt Lake City, Utah, AIAA Paper 2001-3287, 8-11 July, 2001.

[8] Brousseau P., Crête J.-P., Dubois C., Ageing of Polymer-Coated Ultra-Fine Particles, *Paper 89* in *Proceedings of the 36th International Annual Conference of ICT* together with *the 32nd International Pyrotechnics Seminar*, Karlsruhe, Germany, 28 June-1 July, 2005.

[9] Meda L., Marra G., Galfetti L., Severini F., DeLuca L., Nano-aluminum as energetic material for rocket propellants, *Material Science and Engineering C*, Vol. 27, pp. 1393-1396, 2007.

[10] de la Fuente J.L., Fernández-García M., Cerrada M.L., Viscoelastic Behavior in a Hydroxyl-Terminated Polybutadiene Gum and Its Highly Filled Composites: Effect on the Type of Filler on the Relaxation Processes, *Journal of Applied Polymer Science*, Vol. *88*, pp.1705-1712, 2003.

[11] de la Fuente J.L., Rodrìguez O., Dynamic Mechanical Study on the Thermal Aging of a Hydroxyl-Terminated Polybutadiene-Based Energetic Composite, *Journal of Applied Polymer Science*, , Vol. 87, pp. 2397-2405, 2003.

[12] Ramier J., Gauthier C., Chazeau L., Stelandre L., Guy L., Payne Effect in Silica-Filled Styrene-Butadiene Rubber : Influence of Surface Treatment, *Journal of Polymer Science : Part B : Polymer Physics*, Vol. 45, pp. 286-298, 2007.

[13] Tsagaropoulus G., Eisenberg A., Dynamic Mechanical Study of the Factors Affecting the Two Glass Transition Behavior of Filled Polymers. Similarities and Differences with Random Ionomers, *Macromolecules*, Vol. 28, 6067-6077, 1995**.**

[14] Cerri S., Galfetti L., Bohn M.A., Menke K., Ageing Behaviour of HTPB Based Rocket Propellant Formulations, Paper 77 in *Proceedings of the 40th International Annual Conference of ICT*, Karlsruhe, Germany, 23-26 June, 2009.

[15] Raous G., Application of the Christensen-Lo Model to the Reinforcement of Elastomers by Fractal Fillers, *Macromol. Theory Simul.*, Vol. 12, pp. 17-23, 2003.